# Hydroxysteroid (17 beta) dehydrogenase 12 is essential for metabolic homeostasis in adult mice

Heikelä, Hanna

2020-09

## RESEARCH ARTICLE

# Hydroxysteroid (17β) dehydrogenase 12 is essential for metabolic homeostasis in adult mice

**Hanna Heikelä,**[1] **Suvi T. Ruohonen,**[1] **Marion Adam,**[1] **Riikka Viitanen,**[2] **Heidi Liljenbäck,**[1,2] **Olli Eskola,**[2]
**Michael Gabriel,**[1] **Laura Mairinoja,**[1] 🆔 **Alberto Pessia,**[3] **Vidya Velagapudi,**[3] 🆔 **Anne Roivainen,**[1,2,4]
**Fu-Ping Zhang,**[1] **Leena Strauss,**[1] and **Matti Poutanen**[1,5]

[1]*Turku Center for Disease Modeling, Institute of Biomedicine, University of Turku, Turku, Finland;* [2]*Turku PET Centre,
University of Turku, Turku, Finland;* [3]*Institute for Molecular Medicine Finland, University of Helsinki, Helsinki, Finland;*
[4]*Turku PET Centre, Turku University Hospital, Turku, Finland; and* [5]*Department of Internal Medicine, Institute of Medicine,
The Sahlgrenska Academy, University of Gothenburg, Gothenburg, Sweden*

Heikelä H, Ruohonen ST, Adam M, Viitanen R, Liljenbäck H,
Eskola O, Gabriel M, Mairinoja L, Pessia A, Velagapudi V,
Roivainen A, Zhang FP, Strauss L, Poutanen M. Hydroxysteroid
(17β) dehydrogenase 12 is essential for metabolic homeostasis in
adult mice. *Am J Physiol Endocrinol Metab* 319: E494–E508, 2020.
First published July 21, 2020; doi:10.1152/ajpendo.00042.2020.—
Hydroxysteroid 17β dehydrogenase 12 (HSD17B12) is suggested to
be involved in the elongation of very long chain fatty acids. Previously, we have shown a pivotal role for the enzyme during mouse
development. In the present study we generated a conditional
*Hsd17b12* knockout (HSD17B12cKO) mouse model by breeding
mice homozygous for a floxed *Hsd17b12* allele with mice expressing
the tamoxifen-inducible Cre recombinase at the ROSA26 locus. Gene
inactivation was induced by administering tamoxifen to adult mice.
The gene inactivation led to a 20% loss of body weight within 6 days,
associated with drastic reduction in both white (83% males, 75%
females) and brown (65% males, 60% females) fat, likely due to
markedly reduced food and water intake. Furthermore, the knockout
mice showed sickness behavior and signs of liver toxicity, specifically microvesicular hepatic steatosis and increased serum alanine aminotransferase (4.6-fold in males, 7.7-fold in females). The hepatic
changes were more pronounced in females than males. Proinflammatory cytokines, such as interleukin-6 (IL-6), IL-17, and granulocyte
colony-stimulating factor, were increased in the HSD17B12cKO mice
indicating an inflammatory response. Serum lipidomics study showed
an increase in the amount of dihydroceramides, despite the dramatic
overall loss of lipids. In line with the proposed role for HSD17B12 in
fatty acid elongation, we observed accumulation of ceramides, dihydroceramides, hexosylceramides, and lactosylceramides with shorter
than 18-carbon fatty acid side chains in the serum. The results indicate
that HSD17B12 is essential for proper lipid homeostasis and
HSD17B12 deficiency rapidly results in fatal systemic inflammation
and lipolysis in adult mice.

dihydroceramide; lipid; liver; toxicity; weight loss

## INTRODUCTION

Fourteen different hydroxysteroid 17β dehydrogenase
(HSD17B) enzymes have been characterized as enzymes
that have the ability to catalyze the reaction between 17-
ketosteroids and 17β-hydroxysteroids, at least in vitro.
HSD17Bs are encoded by different genes resulting in pro-

teins with distinct amino acid sequences, and they present
with different subcellular localizations as well as varying
cofactor and substrate preferences [see review by Marchais-
Oberwinkler et al. (39)]. All, except HSD17B5, belong to
the very large family of short-chain dehydrogenase/reductase (SDR) enzymes, known for their NAD(H)- or NADP(H)-dependent oxidoreductase activity. Several of the
HSD17B enzymes are involved in the metabolism and
synthesis of various lipids. For example, HSD17B4 is involved in the peroxisomal oxidation of fatty acids (7),
whereas HSD17B8 has been suggested to have a role in
the mitochondrial synthesis of fatty acids (10, 64) and
HSD17B10 is capable for mitochondrial beta-oxidation of
fatty acids (26). HSD17B7 is involved in de novo cholesterol synthesis (32), HSD17B12 is expected to be involved
in long-chain fatty acid elongation (41), and HSD17B13 was
recently shown to be a lipid droplet-associated protein (29)
involved in lipid homeostasis in the liver (1).

HSD17B12 is widely expressed in both human and murine tissues (Fig. 1*A*; see https://genevisible.com/tissues/HS/
UniProt/Q53GQ0 and other expression data banks). The
enzyme was originally characterized as an enzyme converting palmitic acid to arachidonic acid (AA; 41). The view
that HSD17B12 is involved in fatty acid chain elongation is
further supported by several studies. The enzyme expression
was shown to be regulated by sterol regulatory element-binding protein (SREBP), a key regulator of several enzymes involved in lipid metabolism and fatty acid and
cholesterol biosynthesis (42). Furthermore, knockdown of
the *Hsd17b12* expression in cultured SK-BR-3 breast cancer
cells resulted in reduced cell proliferation, whereas the
proliferation was restored by arachidonic acid treatment
(43). Our in vivo study applying a mouse model with a
hypomorphic *Hsd17b12* showed that a reduced expression
of the gene in the ovaries resulted in failure in oogenesis and
ovulation, and the phenotype was associated with a decrease
in the intraovarian concentration of AA and several of its
downstream metabolites, including several prostaglandins
(33). Similarly, the amount of AA was decreased in embryonic stem cells (ESCs) presenting only one functional copy
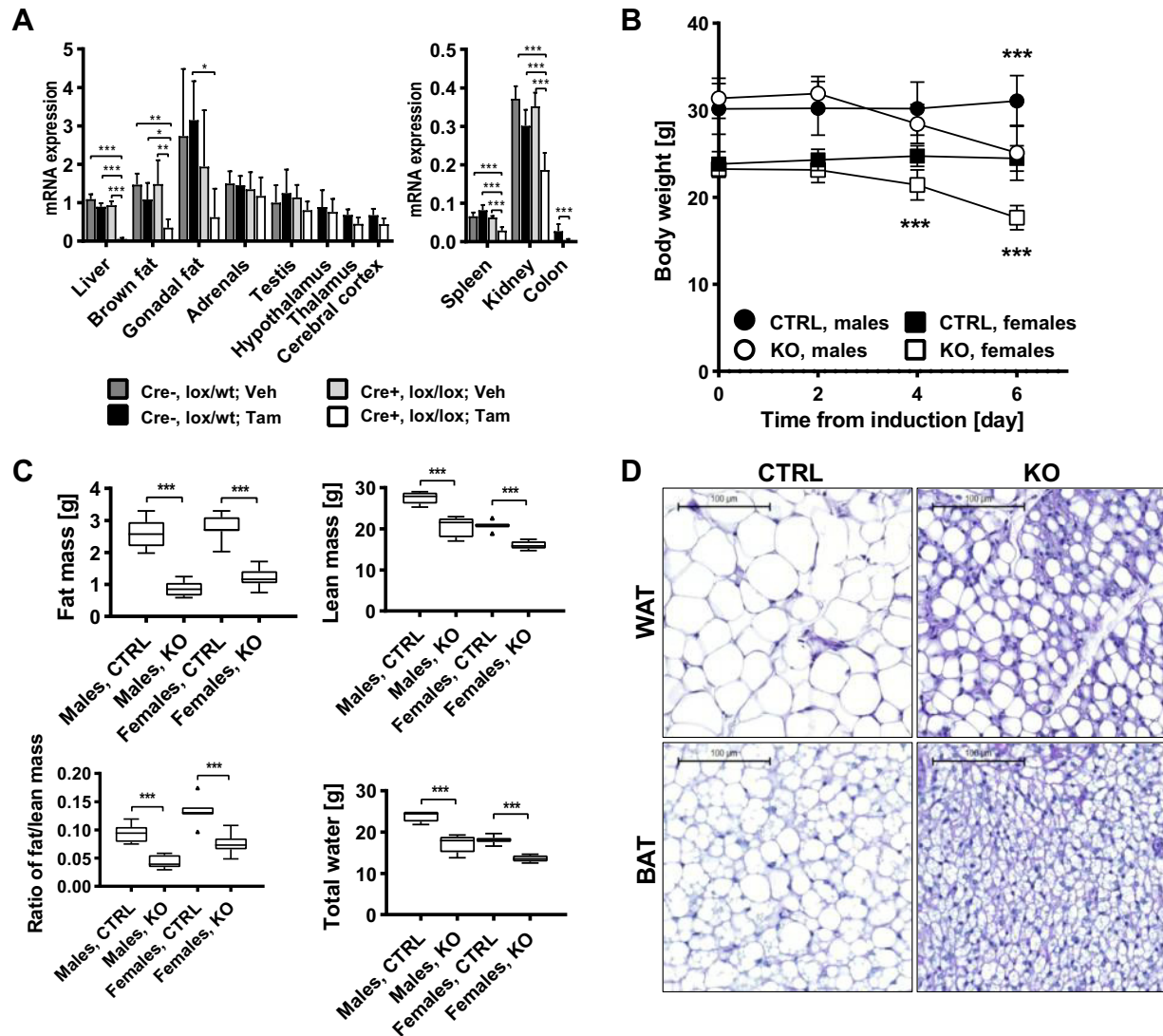of the gene (46).

Fig. 1. Hydroxysteroid 17β dehydrogenase 12 (*Hsd17b12*) expression, body weight, and body composition in mice with induced HSD17B12 deletion in adulthood. *A*: *Hsd17b12* expression in the liver, brown adipose tissue (BAT), gonadal fat, adrenals, testis, hypothalamus, thalamus, cerebral cortex, spleen, kidney, and colon of HSD17B12cKO male mice 6 days postinduction. [Cre− lox/wild type (wt), vehicle (Veh), $n = 3–5$ mice; Cre− lox/wt, tamoxifen (Tam), $n = 3–6$ mice; Cre+ lox/lox, Veh, $n = 4–5$ mice; Cre+ lox/lox, Tam, $n = 4–6$ mice.] Two liver samples of Cre− lox/wt were used as positive controls with every sample set, and the expression level in them was set to 1. The expression levels in other tissues were proportioned to that of the positive controls. The results were analyzed with one-way ANOVA. *B*: the body weight of HSD17B12cKO males and females decreased drastically within 6 days from the induction of Cre recombination. ●, Control (CTRL) males ($n = 10–23$ mice); ○, knockout (KO) males ($n = 17–29$ mice); ■, CTRL females ($n = 7–20$ mice); □, KO females ($n = 7–15$ mice). The CTRL (Cre− lox/wt, Tam) and KO (Cre+ lox/lox, Tam) groups in both sexes were compared with each other at each time point using the *t* test. *C*: body fat mass (*top left*), lean mass (*top right*), ratio of fat mass to lean mass (*bottom left*), and body water content (*bottom right*) of HSD17B12cKO mice on *day 6* compared with the control mice. (Male Cre− lox/wt, Tam, $n = 6$ mice; male Cre+ lox/lox, Tam, $n = 7$ mice; female Cre− lox/wt, Tam, $n = 7$ mice; female Cre+ lox/lox, Tam, $n = 6$ mice.) The CTRL (Cre− lox/wt, Tam) and KO (Cre+ lox/lox, Tam) groups in both sexes were compared with each other using the *t* test. *D*: subcutaneous white adipose tissue (WAT) and BAT depots of 10-wk-old male mice were stained with periodic acid-Schiff (PAS) stain. Subcutaneous white fat (panels at *top*) and brown fat (panels at *bottom*). Scale bars, 100 μm. *$P < 0.05$, **$P < 0.01$, ***$P < 0.001$.

Deleting the *Hsd17b12* gene from the mouse germ line resulted in early embryonic lethality at *embryonic day 9.5* (E9.5) at the latest (4, 46). A more detailed analysis of the knockout (KO) embryos revealed that the embryos initiate gastrulation but their development was disrupted during early organogenesis, indicating that *Hsd17b12* expression is essential for proper embryonic growth and differentiation. More recently, the fatty acid elongation by HSD17B12 has been shown to play a role in the development of inflammation and cancer (14, 34, 43, 66), and in line with these studies,

HSD17B12 was also associated with a poor prognosis of ovarian cancer in a recent genome-wide association study (61). The role of HSD17B12 in ovarian cancer was also indicated by a genome-wide CRISPR/Cas screen of numerous cancer cell lines (3).

In the current study, we aimed to further characterize the in vivo function of HSD17B12 by generating *Hsd17b12* gene deletion in adulthood by utilizing the Cre-lox approach, allowing us to overcome the embryonic lethality observed in mice with the germ line deletion.

## MATERIALS AND METHODS

### Generation of Mouse Lines with Conditional Inactivation of Hsd17b12

The targeting vector for *Hsd17b12* (PGS00030_C_C05) was obtained from the European Conditional Mouse Mutagenesis Program (EUCOMM). In the construct, exon 2 of the *Hsd17b12* gene was flanked by *loxP* sites, and a *lacZ* as well as *neo* cassette was flanked by flippase recognition target (*FRT*) sites. The vector was linearized and electroporated into G4 hybrid mouse embryonic stem cells (G4,

129S6B6F1) for homologous recombination with standard procedures. To identify the properly targeted clones, the colonies were screened with specific primers for the wild-type (wt) and the mutated allele (Table 1). The proper homologous recombination was then confirmed by sequencing. Thereafter, the *lacZ-neo* cassette was removed from the selected ESC clones by flippase (Flp) recombination, and the cells were injected into C57BL/6N mouse blastocysts. The blastocysts were then surgically transferred into pseudopregnant foster mothers (NMRI strain). The resulting chimeric offspring were genotyped and mated with wt C57BL/6NCrl mice to produce the F1

Table 1. *Primers used for genotyping PCR and qRT-PCR assays*

| Target | Strand | Sequence (5′–3′) | Amplicon Size, bp | Annealing T, °C |
|---|---|---|---|---|
| Screening PCR | | | | |
| 17bHSD12Arm5GF2 | For | GCATGCTTCTCTTCTTTGTT | 5,314 | 55.0 |
| 17bHSD12Arm5UR1 | Rev | TACATAGTTGGCAGTGTTTG | | |
| FRse1 | For | GAGATGGCGCAACGCAATTA | 4,597 | 55.0 |
| 17HSD12Arm3GR2 | Rev | GCTGGAAAGGCTTTTGTGTC | | |
| Genotyping PCR | | | | |
| Hsd17b12 | For | TTAGGCTTTACTAGCATATAGC | 206 (wt) | 60.0 |
| | Rev | TATAAGGAAACGGAAGCTCA | 400 (loxP) | |
| Rosa26Cre | For | GCACGTTCACCGCATCAAC | 320 | 60.0 |
| | Rev | CGATGCAACGAGTGATGAGGTTC | | |
| Adipoq-Cre | For | ATACCGGAGATCATGCAAGC | 200 | 58.0 |
| | Rev | GGCCAGGCTGTTCTTCTTAG | | |
| qRT-PCR | | | | |
| Acaca | For | GCCTCTTCCTGACAAACGAG | 239 | 60.0 |
| | Rev | TGACTGCCGAAACATCTCTG | | |
| Acox1 | For | TTATGCGCAGACAGAGATGG | 209 | 61.7 |
| | Rev | AGGCATGTAACCCGTAGCAC | | |
| Agrp | For | CTTTGGCGGAGGTGCTAGAT | 75 | 59.0 |
| | Rev | AGGACTCGTGCAGCCTTACAC | | |
| Cd36 | For | GATGACGTGGCAAAGAACAG | 107 | 59.6 |
| | Rev | TCCTCGGGGTCCTGAGTTAT | | |
| Cpt1a | For | CCAGGCTACAGTGGGACATT | 209 | 57.0 |
| | Rev | GAACTTGCCCATGTCCTTGT | | |
| Crh | For | ACTCAGAGCCCAAGTACGTT | 164 | 60.9 |
| | Rev | GCTCTCTTCTCCTCCCTTGG | | |
| Dgat1 | For | GCCACAATCATCTGCTTCCC | 190 | 60.0 |
| | Rev | CCACTGACCTTCTTCCCTGT | | |
| Dgat2 | For | CCAAGAAAGGTGGCAGGA | 174 | 60.0 |
| | Rev | TGAAGTTACAGAAGGCACCC | | |
| Fasn | For | TGGGTTCTAGCCAGCAGAGT | 158 | 59.0 |
| | Rev | ACCACCAGAGACCGTTATGC | | |
| Fatp2 | For | ATGCCGTGTCCGTCTTTTAC | 168 | 59.6 |
| | Rev | GACCTGTGGTTCCCGAAGTA | | |
| G6pc | For | CTGTTTGGACAACGCCCGTAT | 91 | 61.8 |
| | Rev | AGGTGACAGGGAACTGCTTTA | | |
| L19 | For | GGACAGAGTCTTGATGATCTC | 195 | 60.0 |
| | Rev | CTGAAGGTCAAAGGGAATGTG | | |
| Npy | For | CCGCTCTGCGACACTACAT | 68 | 60.9 |
| | Rev | TGTCTCAGGGCTGGATCTCT | | |
| Pepck | For | CTGAAGGTGTCCCCCTTGTC | 110 | 59.6 |
| | Rev | GATCTTGCCCTTGTGTTCTGC | | |
| Pklr | For | TGGCATCGAAAGTGGAAAGC | 193 | 60.9 |
| | Rev | GATGTGGGACTATGGGAGGG | | |
| Pomc | For | CAAGCCGGTGGGCAAGAAACG | 119 | 60.9 |
| | Rev | CTAATGGCCGCTCGCCTTCCAG | | |
| Ppara | For | ATGCCAGTACTGCCGTTTTC | 220 | 61.8 |
| | Rev | GGCCTTGACCTTGTTCATGT | | |
| Ppia | For | CATCCTAAAGCATACAGGTCCTG | 165 | 60.0 |
| | Rev | TCCATGGCTTCCACAATGTT | | |
| Scd1 | For | CATTCTCATGGTCCTGCTGC | 163 | 59.6 |
| | Rev | TGCCTTGTAAGTTCTGTGGC | | |

Here, bp, base pairs; For, forward; qRT-PCR, quantitative RT-PCR; Rev, reverse; T, temperature; wt, wild type. Acaca, acetyl-CoA carboxylase-α; Acox1, acyl-CoA oxidase 1; Agrp, agouti-related peptide; Cd36, cluster of differentiation 36; Cpt1a, carnitine palmitoyl transferase 1; Crh, corticotropin-releasing hormone; Dgat1 and Dgat2, diacylglycerol O-acyltransferase 1 and 2, respectively; Fasn, fatty acid synthase; Fatp2, fatty acid transport protein 2; G6pc, glucose-6-phosphatase L19, ribosomal protein L19; Npy, neuropeptide Y; Pepck, phosphoenolpyruvate carboxykinase; Pklr, pyruvate kinase L/R, Pomc, proopiomelanocortin; Ppara, peroxisome proliferator-activated receptor-α; Ppia, peptidylprolyl isomerase A; Scd1, acyl-CoA desaturase 1.

generation to test the germ line transmission. The mouse colony was maintained by using the heterozygous littermates in breeding. A schematic representation of the targeted, floxed, and deleted allele is shown in Supplemental Fig. S1*A* (all Supplemental Material is available at https://doi.org/10.6084/m9.figshare.12465512). The presence of the wt and/or mutated *Hsd17b12* gene in mice was analyzed by PCR (Table 1 and Supplemental Fig. S1*B*). The mice with the floxed allele were crossed with the Rosa26CreER$^T$ strain (67) to generate a tamoxifen (Tam)-inducible conditional KO mouse strain (HSD17B12cKO; Supplemental Fig. S1*C*). The primer pair used to identify the presence of Rosa26Cre-ER$^T$ alleles is listed in Table 1. The adipocyte-specific, tamoxifen-inducible conditional KO mouse strain (aHSD17B12cKO; Supplemental Fig. S1*D*) was generated by breeding the HSD17B12-loxP mice with AdipoqCreER$^{T2}$ mice (51). The primers used for genotyping the presence of the Cre-ER$^{T2}$ gene in these mice are shown in Table 1.

Gene deletions in both KO models were induced by daily intraperitoneal injections of 1.5 mg tamoxifen (Sigma-Aldrich, St. Louis, MO) for 5 consecutive days. Tamoxifen was dissolved in ethanol and then diluted 1:10 in rapeseed oil. Ethanol diluted in rapeseed oil was used as a vehicle.

All animal handling was conducted under animal license no. 10605/04.10.07/2016, granted by the Animal Experiment Board in Finland, and was performed in accordance with the institutional animal care policies, which fully meet the requirements defined in the National Institutes of Health (Bethesda, MD) guidelines on animal experimentation. Animals were housed at the Central Animal Laboratory at the University of Turku, Turku, Finland, in individually ventilated cages (IVCs; Techniplast, Buguggiate, Italy) with ~70 air changes per hour and with constant temperature at $21 \pm 3°C$ and humidity at $55 \pm 15\%$ [means $\pm$ standard deviation (SD)]. A 12:12-h light-dark cycle was applied, with a light change at 7 AM and 7 PM. Autoclaved aspen chips were used as bedding (Tapvei Ltd., Harjumaa, Estonia), and soy-free pellets (RM3; Special Diets Services, Essex, UK) and water were available ad libitum. Every cage had a nest box, and tissue paper was provided for nest building. The animals were individually identified with ear marks and housed with littermates (1–6 mice per cage). Animals were euthanized with $CO_2$ asphyxiation and cervical dislocation.

### Analyzing the Body Weight, Body Composition, and Weight of the Adipose Tissue Depots

*HSD17B12cKO.* The body weight of the HSD17B12cKO mice was monitored for 7 days by weighing the mice once a day, starting at the time of the last Tam injection (*day 0*). Body composition (lean mass, fat mass, and free water) was measured using an EchoMRI-700 device (Echo Medical Systems, Houston, TX) in live mice on *day 6* after the last Tam injection. At the time of necropsy (6 days after the last Tam injection) the weight of the various white adipose tissue (WAT) depots (subcutaneous, gonadal, and perirenal), brown adipose tissue (BAT), and various organs (liver, spleen, kidneys, adrenals, pancreas, pituitaries, and heart) was measured, and tissues were collected in liquid nitrogen and formalin.

*aHSD17B12cKO.* The body weight and composition of the aHSD17B12cKO mice were monitored for 3 mo by weighing the mice and performing the EchoMRI analyses once a month. The mice were euthanized at the age of 5 mo, and interscapular BAT, subcutaneous, gonadal, and perirenal adipose tissue, and liver were collected in liquid nitrogen and formalin.

### Histological Analysis

For hematoxylin-eosin (H&E) or periodic acid-Schiff (PAS) staining, tissues collected at the time of necropsy were dissected and fixed in 10% buffered formalin at room temperature for 24–48 h, dehydrated with increasing ethanol concentrations and xylene, and embedded in paraffin. After deparaffinization and rehydration, 4-μm-thick sections were stained with H&E or PAS for microscopic analysis. For Oil Red O (ORO) staining, the tissue samples were embedded in Tissue-Tek O.C.T. (Sakura Finetek USA, Inc., Torrance, CA) and frozen in 2-methylbutane cooled with dry ice. Then 8-μm-thick sections were cut and stained with ORO (Sigma-Aldrich). Microscope slides were scanned using a Pannoramic 250 Flash digital slide scanner (3DHISTECH Ltd., Budapest, Hungary).

### Quantification of Apoptotic Cells in the Liver

Four-micrometer-thick paraffin sections of the liver from HSD17B12cKO and control (CTRL) mice (males, CTRL $n = 7$ mice and KO $n = 7$ mice; females, CTRL $n = 6$ mice and KO $n = 8$ mice) were deparaffinized and rehydrated. Antigen retrieval was performed in a microwave in citrate buffer (pH 6.0). Endogenous peroxidase activity was inhibited by 3% $H_2O_2$. The sections were then incubated in the terminal deoxynucleotidyl transferase (TdT) dUTP nick end labeling (TUNEL) reaction mixture containing TdT and biotin-16-dUTP (Roche Diagnostics GmbH) at 37°C for 1 h. The reaction was terminated by adding 300 mM NaCl over the sections. The sections were then blocked with 3% bovine serum albumin (BSA) and incubated in ExtrAvidine (Sigma-Aldrich, diluted 1:500 in 1% BSA) for 30 min at 37°C, followed by staining with 3,3′-diaminobenzidine (Dako Liquid DAB+ Substrate Choromogen System; Dako North America, Carpinteria, CA). Finally, the sections were counterstained with Mayer's hematoxylin, dehydrated, and mounted.

Slides were scanned using a Pannoramic 250 Flash digital slide scanner (3DHISTECH Ltd., Budapest, Hungary). Digital slide images were then imported into QuPath, version 0.2.0, an open-source software platform (2). Apoptotic cells were identified using the positive cell detection feature of QuPath, which detects the nuclei and classifies them as positive (apoptotic cells) or negative with QuPath's built-in cell segmentation algorithms. The analysis was performed on one sagittal section of the left lateral lobe per animal (mean area 52.2 mm$^2$). A total of three outliers were excluded by the ROUT method in GraphPad Prism (GraphPad Software, La Jolla, CA) with coefficient $Q = 1\%$ from male CTRL, male KO, and female CTRL groups, one from each group. The mean percentage of positive nuclei of all detected nuclei was compared between the control and KO groups.

### Adipocyte Size

PAS-stained adipose tissue slides were scanned for further analysis with a Pannoramic 250 Flash series digital slide scanner (3DHISTECH Ltd.). Three to four ×10 images were taken with 3DHISTECH CaseViewer version 2.3. AdipoCount software (74) was used to measure the average adipocyte size in the images for each animal.

### Triglyceride Measurement

Frozen liver samples were homogenized in PBS containing 0.1% Nonidet P-40 (Roche Diagnostics GmbH) with TissueLyser LT (Qiagen, Hilden, Germany) using 5-mm stainless steel beads at 50 Hz for 2 min. After homogenization, the samples were incubated on ice for 30 min and spun down for 2 min at 12,000 relative centrifugal force (RCF). Triglyceride concentration was measured in the supernatants with Serum Triglyceride Determination Kit (Sigma-Aldrich) according to the manufacturer's instructions, scaled down for 96-well plates. The absorbance was measured with an EnSight multimode plate reader (PerkinElmer, Waltham, MA).

### Analyzing the mRNA Expression

RNA was extracted from frozen tissues with TRIsure (Bioline, London, UK) and treated with Amplification Grade DNase I (Sigma-Aldrich). One microgram of RNA was then reverse transcribed using SensiFAST cDNA Synthesis Kit (Bioline), and mRNA levels were analyzed by quantitative RT-PCR using Dynamo Flash SYBR Green

qPCR Kit (Thermo Fisher Scientific, Waltham, MA) and the CFX96 Real-Time C1000 Thermal Cycler (Bio-Rad, Hercules, CA). Standards were run in duplicate, and all RNA samples for the genes of interest as well as reference genes [ribosomal protein L19 (*L19*) and peptidylprolyl isomerase A (*Ppia*)] used for normalization were analyzed in triplicate. Sequences of the primers used are listed in Table 1.

*Clinical Chemistry Analyses of the Blood*

Various clinical chemistry parameters were analyzed in seven control (Cre− lox/lox) and six HSD17B12cKO (Cre+ lox/lox) male mice as well as in five control (Cre− lox/lox) and five (Cre+ lox/lox) female mice on *day 6* after Tam induction. Approximately 110 μL of whole blood were collected from the saphenous vein in BD Microtainer lithium-heparin blood collection tubes (Becton, Dickinson and Company, Franklin Lakes, NJ) and analyzed for albumin, alkaline phosphatase, alanine aminotransferase (ALT), amylase, blood urea nitrogen, total calcium, creatinine, globulin, glucose, potassium, sodium, phosphate, total bilirubin, and total protein concentrations using a Comprehensive Diagnostic Profile rotor (Abaxis, Inc., Union City, CA) and Vetscan VS2 analyzer (Abaxis, Inc.).

*Lipidomics Analysis in the Serum*

For lipidomic studies, blood was collected from five control (Cre−, lox/lox) and five HSD17B12cKO (Cre+, lox/lox) males, 6 days post-Tam induction via heart puncture, allowed to coagulate overnight at +4°C, and spun down to extract serum. Thereafter, quantitative lipidomic analysis was performed as described earlier (23). Shortly, lipids were extracted with liquid-liquid extraction using ethyl acetate and methanol. To a 100-μL serum sample, 1 mL methanol, 1 mL water, and 100 μL of labeled internal lipid standards were added, and lipids were extracted by adding 3.5 mL of ethyl acetate. Dried samples were reconstituted with 250 μL of mobile phase (dichloromethane-methanol; 50:50, containing 10 mM ammonium acetate) for injection. Lipid separation and quantitation was performed on the SCIEX Lipidyzer platform using a SCIEX 5500 QTRAP mass spectrometer (SCIEX, Framingham, MA) with SelexION differential ion mobility (DMS) technology. The lipid molecular species were measured using the multiple reaction monitoring (MRM) strategy in both positive and negative polarities. Positive ion mode was used for the detection of lipid classes dihydroceramides (DCERs), hexosylceramides (HCERs), lactosylceramides (LCERs), sphingomyelins (SMs), diacylglycerols (DAGs), cholesteryl esters (CEs), ceramides (CERs), and triacylglycerols (TAGs), and negative ion mode was used for the detection of lipid classes lysophosphatidylethanolamines (LPEs), lysophosphatidylcholines (LPCs), phosphatidylcholines (PCs), phosphatidylethanolamines (PEs), and free fatty acids (FFAs). Lipidomics Workflow Manager software (SCIEX) was used for acquisition of samples, automated data processing, signal detection, and lipid species concentration calculations. Data analysis was performed with MetaboAnalyst 4.0 (11). A total of 856 lipids were analyzed, of which 222 lipids contained missing values. Of these, 137 lipids were found to have missing values in at least 40% of samples (2 samples) in both KO and control mice and were, therefore, discarded before the statistical analysis. Missing values from the remaining 85 lipids were input using the MissForest package (60). Values were log transformed, and no outliers were observed.

*Measuring Serum Cytokines*

Blood was collected via heart puncture from 10 control (Cre−, lox/lox) and 10 HSD17B12cKO (Cre+, lox/lox) males as well as 9 control (Cre−, lox/lox) and 10 HSD17B12cKO (Cre+, lox/lox) females on *day 6* post-Tam induction. To separate serum, blood was allowed to coagulate overnight at +4°C and spun down. Cytokine levels were measured using Luminex 200 with xPONENT 3.1. software (Luminex, Austin, TX) and MILLIPLEX MAP Mouse Cyto-

kine/Chemokine Magnetic Bead Panel (MCYTOMAG-70K-PMX; Merck Millipore, Billerica, MA) according to the manufacturer's protocol. The cytokines measured included granulocyte colony-stimulating factor (G-CSF), granulocyte-macrophage colony-stimulating factor (GM-CSF), interferon-γ (IFN-γ), interleukin-1α (IL-1α), IL-1B, IL-2, IL-4, IL-5, IL-6, IL-7, IL-9, IL-10, IL-12 (p40), IL-12 (p70), IL-13, IL-15, IL-17, interferon-γ-induced protein 10 (IP-10), keratinocyte chemoattractant (KC), monocyte chemoattractant protein 1 (MCP-1), macrophage inflammatory protein 1-α (MIP-1α), MIP-1β, MIP-2, regulated on activation, normal T cell expressed and secreted (RANTES), and tumor necrosis factor-α (TNF-α). The minimum detectable concentrations were 3.2 pg/mL for all the cytokines except 12.8 pg/mL for IL-13.

*Indirect Calorimetry*

Six control (Cre− lox/lox) and six HSD17B12cKO (Cre+ lox/lox) males were placed (1 mouse per cage) in OxyletPro indirect calorimetry cages (Panlab, S.L.U., Barcelona, Spain) 3 days after the first Tam injection. The system analyzes changes in $O_2$ and $CO_2$ concentrations, and its high-precision extensiometric weight transducer measures water consumption. In addition, the sensor platform records spontaneous activity and rearing events to determine activity levels. The measurement (3 days) was conducted between *days 3* and *5* post-Tam induction.

*Measuring Food Consumption*

Three control (Cre− lox/lox) and five HSD17B12cKO (Cre+ lox/lox) males were housed in individual cages. To determine the amount of food consumed, food pellets were weighed before and after the measurement period on the morning of *day 0* (after the last Tam injection) and then every 24 h until *day 5* post-Tam induction.

*2-[18F]Fluoro-2-deoxy-D-glucose Positron Emission Tomography Studies*

To standardize blood glucose level, mice were fasted for 3 h with ad libitum access to water before 2-[18F]fluoro-2-deoxy-D-glucose ([18F]FDG) injection. The blood glucose concentrations were measured using a glucometer (Bayer Contour; Bayer, Leverkusen, Germany) before and after [18F]FDG PET/computed tomography (CT) imaging. For PET/CT imaging, the mice were anesthetized using isoflurane (3–4% induction and 1–2% maintenance), and the tail vein was cannulated. The mice were intravenously injected with 5.1 ± 0.1 MBq of [18F]FDG and scanned using a small-animal PET/CT (Inveon Multimodality; Siemens Medical Solutions, Knoxville, TN) for 60 min starting from the time of the injection. The PET data acquired in a list mode were iteratively reconstructed with an ordered subset expectation maximization three-dimensional (3-D) algorithm, followed by maximum a posteriori reconstruction. Quantitative PET image analysis was performed using Carimas 2.9 software (Turku PET Centre). The regions of interest were defined in brain, heart, kidney, liver, lung, muscle, and urinary bladder using CT as the anatomical reference. The uptake of [18F]FDG was reported as a standardized uptake value (SUV), which takes into account animal weight and injected radioactivity dose. Immediately after PET/CT, blood was collected via cardiac puncture under terminal isoflurane anesthesia, and mice were euthanized by cervical dislocation; various tissues were excised and weighed, and their total radioactivity was measured using a gamma counter (Triathler 3 in.; Hidex Oy, Turku, Finland). The results are expressed as SUV.

*Statistical Analysis*

Statistical analyses were performed using GraphPad Prism 8.1.2 software (GraphPad Software, La Jolla, CA). Outliers were identified using the ROUT method in Prism with coefficient $Q = 1\%$. The Shapiro–Wilk test was used to test for normal distribution. The statistical tests were chosen depending on the results of the Shapiro–Wilk tests of data normality. If not otherwise indicated, unpaired *t* test

or nonparametric Mann–Whitney test was used to determine the statistical significance between two groups at a single time point, and two-way ANOVA was used for multiple time points. For adipocyte size and *Hsd17b12* mRNA expression, the statistical significance was analyzed by one-way ANOVA. The threshold for statistical significance was set at $P < 0.05$. Results are expressed as means ± SD, unless otherwise indicated.

## RESULTS

### *Inducing Hsd17b12 Gene Inactivation in Adulthood Results in Dramatic Weight Loss*

In the HSD17B12cKO mouse model, the exon 2 deletion was initiated at the age of 8 wk by injecting 1.5 mg of Tam per day for 5 consecutive days. This resulted in a marked decrease in *Hsd17b12* mRNA levels in the different tissues measured 6 days after Tam injection, whereas with vehicle injection no effect on the mRNA expression was observed (Fig. 1*A*). This confirmed the Tam dependency of the gene deletion. The strongest reduction in the mRNA level was observed in the liver with a drop of 94%, followed by the colon (85%), the WAT (77%), and the BAT (76%). Also in the kidney (50%) and spleen (56%) a significant reduction was observed. In the different brain regions and adrenals the mRNA levels were not reduced significantly 6 days after completing the Tam treatment (Fig. 1*A*), despite the confirmed expression of tamoxifen-inducible Cre recombinase. The reason for phenotyping the mice only 6 days after the initiation of the gene deletion was that both the male and female HSD17B12cKO mice were dramatically losing body weight during these 6 days (Fig. 1*B*), and at *day 6* the weight was reduced 17% in males (KO *day 0*, 30.3 ± 1.45 g; KO *day 6*, 25.1 ± 3.17 g) and 24% in females (KO *day 0*, 23.2 ± 0.95 g; KO *day 6*, 18.1 ± 1.59 g). No effect on body weight during the study period was observed in the Tam-treated controls lacking the Cre or expressing one wt allele. The weight loss was especially severe from *day 4* to *day 6*. The physical appearance and behavior of the HSD17B12cKO mice were normal until *day 6*, whereas at *day 6* the mice sat hunched and showed other signs of general indisposition, and thus, the study period could not be extended. As analyzed by EchoMRI, the weight loss was accompanied with drastically lower fat content in the HSD17B12cKO mice compared with the Tam-treated controls in both females and males (56% and 66% lower, respectively; Fig. 1*C*). The reduced fat mass was confirmed ex vivo by analyzing the weights of the different adipose tissue depots (Supplemental Fig. S2). The reduced amount of fat in the HSD17B12cKO mice was also associated with reduced lipid droplet size in both the WAT and BAT in HSD17B12cKO mice compared with controls (Fig. 1*D*). The loss of fat tissue was accompanied by a significant loss of the lean mass (23% in females and 25% in males).

### *The Weight Loss in HSD17B12cKO Mice Is Caused by Reduced Water and Food Intake, whereas the Hypothalamic Regulation of Feeding Is Intact*

To define the cause of the rapid loss of adipose tissue, we first assessed the overall energy consumption of HSD17B12cKO males. The data indicated that energy consumption of the HSD17B12cKO mice did not differ from that of the control mice when normalized to the lean mass (Sup-

plemental Fig. S3*A*). Therefore, the results indicate that the weight loss was not primarily due to an increased metabolic rate of the HSD17B12cKO mice. Neither was there a difference in the locomotor activity (Supplemental Fig. S3*B*) or in the number of rearing events (Supplemental Fig. S3*C*) between the HSD17B12cKO and the control mice. However, HSD17B12cKO males show a decreased respiratory exchange ratio during *day 4*, indicating a switch from using carbohydrates as the fuel source to burn fat (Supplemental Fig. S3*D*). While measuring the water and food intake, we observed that the HSD17B12cKO mice drastically reduced water consumption during *days 3–5* after Tam induction (Fig. 2*A*) and the caloric intake was markedly reduced during *days 2–5*
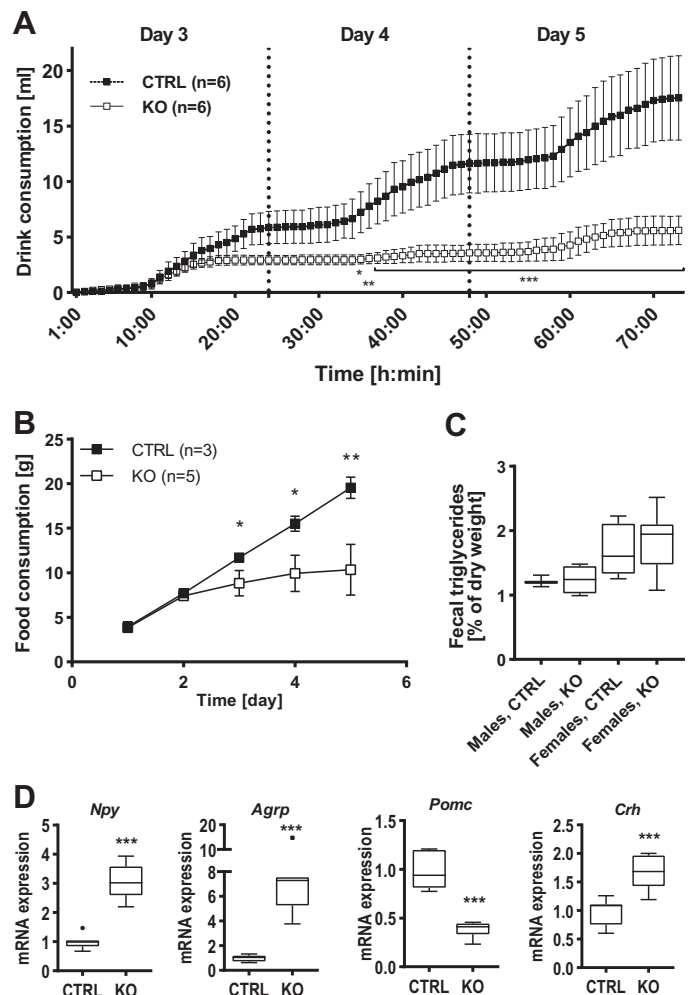


Fig. 2. Water and food consumption of conditional hydroxysteroid 17β dehydrogenase 12 knockout (HSD17B12cKO) mice. *A*: cumulative water consumption of males during *days 3–5* postinduction. Two-way ANOVA. *B*: cumulative food consumption of males during *days 1–5* postinduction. Two-way ANOVA. *C*: lipid content in feces of control (CTRL) and HSD17B12cKO (KO) mice. [Male CTRL, tamoxifen (Tam), *n* = 3 mice; male KO, Tam, *n* = 4 mice; female CTRL, Tam, *n* = 7 mice; female KO, Tam, *n* = 7 mice.] The CTRL and KO groups in both sexes were compared with each other using the *t* test. *D*: relative mRNA expression levels of genes regulating hunger-signaling [neuropeptide Y (*Npy*) and agouti-related peptide (*Agrp*)] as well as satiety-signaling genes [proopiomelanocortin (*Pomc*) and corticotropin-releasing hormone (*Crh*)] in CTRL and KO female mice on *day 6* postinduction in the hypothalamus. *t* Test. (CTRL, Cre− lox/lox, Tam, *n* = 8 mice; KO, Cre+ lox/lox, Tam, *n* = 7–8 mice.) *P < 0.05, **P < 0.01, ***P < 0.001.

postinduction (Fig. 2*B*). The control males consumed 3.7–4.0 g of chow per day, whereas the HSD17B12cKO males consumed only 0.4–1.4 g/day, resulting in significantly reduced food consumption over the study period ($P < 0.004$), also indicated by lower serum glucose levels in KO mice compared with controls (Table 2). Increased levels of serum albumin and total proteins in HSD17B12cKO mice compared with the controls, measured on *day 6* postinduction, indicated severe dehydration of HSD17BcKO mice (Table 2). The lipid contents in the feces of KO mice did not differ from those of the control mice, suggesting that the weight loss was not due to fat malabsorption in the KO mice (Fig. 2*C*). These data prompted us to assess the expression levels of the genes mediating the satiety and hunger signals in the hypothalamus. mRNAs for major hunger-inducing signaling components, such as neuropeptide Y (*Npy*) and agouti-related peptide (*Agrp*), were upregulated, whereas for those regulating satiety, proopiomelanocortin (*Pomc*) was downregulated, and corticotropin releasing hormone (*Crh*) was upregulated in the HSD17B12cKO mice compared with the control mice (Fig. 2*D*). Using [$^{18}$F]FDG PET imaging, both in vivo and ex vivo results (Supplemental Fig. S4) indicated a normal, or slightly increased, glucose uptake in the brain of HSD17B12cKO mice compared with the controls. These results suggest that the hypothalamic regulation of feeding is responsive to the weight loss condition and that the observed metabolic defect is not of hypothalamic origin.

### HSD17B12 Expression in the Adipocytes Is Not Essential for Metabolic Homeostasis

We also investigated whether the significantly reduced *Hsd17b12* expression detected in the adipose tissue of the HSD17B12cKO (Fig. 1*A*) initiates the observed metabolic disturbance. For this purpose, we generated an inducible adipocyte-specific HSD17B12 KO mouse model (aHSD17B12cKO). The gene deletion in the adipocytes was induced by a 5-day-long Tam treatment at the age of 8 wk, followed by the analysis of body weight and body composition of the mice. However, within 6 days after Tam treatment no alteration in body weight or fat content was observed. Neither did we observe a pheno-

type similar to that of the HSD17B12cKO mice at any of the later time points, despite a marked decrease in *Hsd17b12* mRNA expression in the adipocytes (Fig. 3*A*). Three months after the Tam injection, the aHSD17B12cKO mice presented with a body fat mass and lean mass similar to those of the control mice (Fig. 3, *B*–*D*). Furthermore, the lipid droplets within adipocytes did not appear smaller in the aHSD17B12cKO mice than in the control mice (Fig. 3*E*). These results indicated that the loss of HSD17B12 activity in the adipocytes in adult mice does not lead to the severe metabolic alteration and starvation that was observed in the HSD17B12cKO mice.

### Inducing Hsd17b12 Gene Inactivation in Adulthood Results in Altered Serum Lipid Profile, Liver Steatosis, and Signs of General Toxicity

We next performed serum lipidomic analysis to obtain a more detailed understanding of the consequences of the *Hsd17b12* disruption on circulating lipids in HSD17B12cKO mice. As expected, and shown by the heat map (Fig. 4*A*), the majority of the 872 metabolites of 13 different lipid classes measured were at markedly lower levels in the HSD17B12cKO mice, although some lipid species accumulating in the KO mice were identified as well. The genotypes completely segregated into separate clusters according to the phenotype. The volcano plot (Fig. 4*B*) shows that TAGs were the most severely decreased lipid class, but CERs, LPEs, LPCs, PCs, SMs, and LCERs were also significantly decreased in HSD17B12cKO serum compared with controls. Interestingly, the HSD17B12cKO serum showed a 1.39-fold higher concentration of DCERs [$\log_2(1.39) = 0.48$; Fig. 4*B*] compared with controls, DCERs being the only lipid class found to accumulate during the weight loss. As the total amount of ceramides was markedly reduced, the DCER-to-CER ratio (DCER/CER) was increased by 2.6-fold (CTRL, DCER/CER = 0.16; KO, DCER/CER = 0.42), with the highest increase in the concentration of DCER(FA16:0). In all groups of ceramides (CERs, DCERs, LCERs, and HCERs), we also observed an increased relative amount of fatty acids with chain length of 14 and 16 carbon atoms (FA14:0 and FA16:0) and a reduced amount of fatty acids with longer chain lengths (FA18:0, FA20:0, FA22:0 and

**Table 2.** *Clinical chemistry results from whole blood of HSD17B12cKO mice*

| Parameter | Males | | | | Females | | | |
|---|---|---|---|---|---|---|---|---|
| | Control | HSD17B12cKO | FC | P Value | Control | HSD17B12cKO | FC | P Value |
| *n* | 7 | 6 | | | 5 | 5 | | |
| Albumin, g/L | 40.7 ± 2.43 | 46.8 ± 3.49 | 1.15 | 0.017† | 46.2 ± 1.30 | 50.8 ± 3.06 | 1.10 | 0.013† |
| Alkaline phosphatase, U/L | 134 ± 25.1 | 186 ± 37.5 | 1.39 | 0.024† | 198 ± 23.4 | 180 ± 27.4 | 0.91 | 0.429 |
| Alanine aminotransferase, U/L | 27.3 ± 5.96 | 126 ± 120 | 4.63 | 0.190 | 22.0 ± 2.73 | 170 ± 66.6 | 7.71 | 0.004‡ |
| Amylase, U/L | 827 ± 52.9 | 870 ± 163 | 1.05 | 0.485 | 715 ± 34.4 | 653 ± 144 | 0.91 | 0.429 |
| Total bilirubin, μmol/L | 4.57 ± 0.79 | 4.80 ± 0.84 | 1.05 | 0.665 | 4.40 ± 0.54 | 5.00 ± 1.00 | 1.14 | 0.357 |
| Blood urea nitrogen, mmol/L | 7.66 ± 0.69 | 14.1 ± 14.3 | 1.84 | 0.394 | 6.84 ± 1.08 | 15.2 ± 13.9 | 2.23 | 0.011† |
| Total calcium, mmol/L | 2.51 ± 0.05 | 2.52 ± 0.08 | 1.01 | 0.732 | 2.56 ± 0.04 | 2.62 ± 0.03 | 1.02 | 0.050† |
| Phosphate, mmol/L | 2.95 ± 0.45 | 2.03 ± 0.46 | 0.69 | 0.026† | 2.37 ± 0.36 | 2.31 ± 0.44 | 0.98 | 0.931 |
| Creatinine, μmol/L | 23.1 ± 5.58 | 29.3 ± 11.6 | 1.27 | 0.446 | 25.6 ± 7.76 | 22.5 ± 7.15 | 0.88 | 0.307 |
| Glucose, mmol/L | 8.71 ± 1.55 | 5.33 ± 3.24 | 0.61 | 0.071 | 8.12 ± 1.36 | 5.13 ± 2.00 | 0.63 | 0.017† |
| Sodium, mmol/L | 148 ± 1.89 | 149 ± 2.40 | 1.01 | 0.316 | 148. ± 2.68 | 154 ± 3.44 | 1.04 | 0.022† |
| Potassium, mmol/L | 6.26 ± 0.81 | 5.78 ± 0.67 | 0.92 | 0.452 | 5.90 ± 1.13 | 6.23 ± 1.19 | 1.06 | 0.875 |
| Total protein, g/L | 58.1 ± 2.54 | 65.7 ± 5.72 | 1.13 | 0.039† | 60.2 ± 1.64 | 66.3 ± 4.97 | 1.10 | 0.015† |
| Globulins, g/L | 17.1 ± 2.19 | 18.8 ± 2.56 | 1.10 | 0.290 | 14.0 ± 0.71 | 15.7 ± 2.73 | 1.12 | 0.221 |

Values are means ± SD; *n* = no. of mice. FC, fold change; HSD17B12cKO, conditional hydroxysteroid 17β dehydrogenase 12 knockout. †$P < 0.05$, ‡$P < 0.001$, significantly different results.
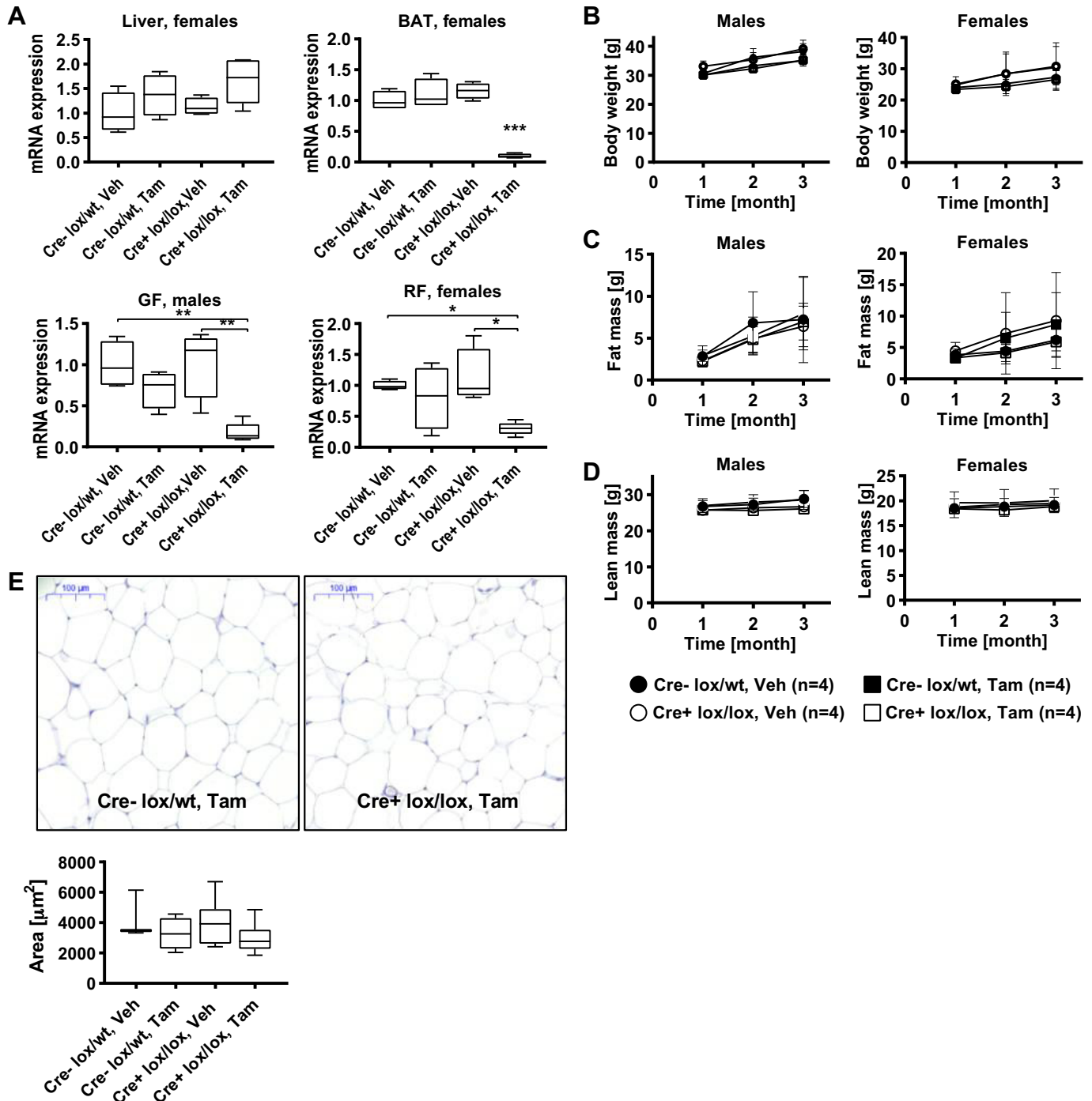
Fig. 3. Body composition of the adipocyte-specific conditional hydroxysteroid 17β dehydrogenase 12 knockout (HSD17B12cKO) mice. A: *Hsd17b12* expression in the liver, brown fat [brown adipose tissue (BAT)], gonadal fat (GF), and perirenal fat (RF). [Cre− lox/wt, vehicle (Veh), $n = 4$ mice; Cre− lox/wt, tamoxifen (Tam), $n = 4$ mice; Cre+ lox/lox, Veh, $n = 4$ mice; Cre+ lox/lox, Tam, $n = 5$ mice.] One-way ANOVA. B–D: body weight (B), body fat mass (C), and lean mass (D) of males and females. Two-way ANOVA. E: gonadal fat of 5-mo-old males stained with hematoxylin-eosin (H&E) and mean adipocyte size in gonadal fat of male mice. (Cre− lox/wt, Veh, $n = 3$ mice; Cre− lox/wt, Tam, $n = 4$ mice; Cre+ lox/lox, Veh, $n = 4$ mice; Cre+ lox/lox, Tam, $n = 6$ mice.) Scale bars, 100 μm. One-way ANOVA. $*P < 0.05$, $**P < 0.01$, $***P < 0.001$.

22:1, and FA24:0 and 24:1; Fig. 4C). This strongly suggests a defect in the fatty acid elongation in the HSD17B12cKO mice. To our surprise, we did not observe any specific changes in the AA levels as a free form or as a component of the various lipid classes.

Six days after the Tam injection we observed significant fat accumulation in the livers of female HSD17B12cKO mice

(Fig. 5, A and C). Fat accumulation was observed in some HSD17B12cKO male mice as well, but the difference in the amount of triglycerides between the control males and HSD17B12cKO males did not reach statistical significance. The liver injury in HSD17B12cKO mice was further supported by 8-fold-increased ($P < 0.005$) and 5-fold-increased serum
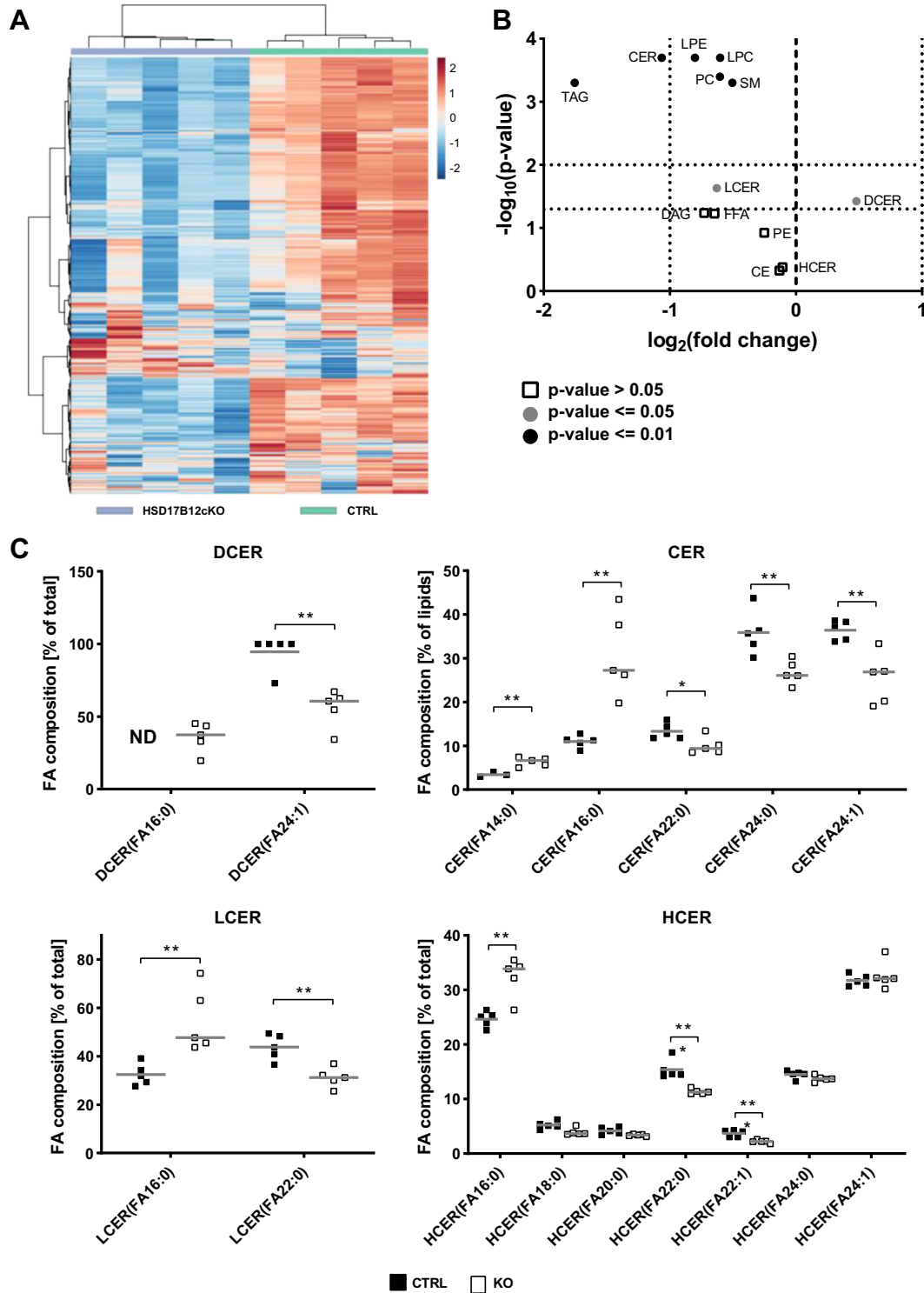
Fig. 4. Serum lipidomics of conditional hydroxysteroid 17β dehydrogenase 12 knockout (HSD17B12cKO) males on *day 6* after tamoxifen (Tam) induction. *A*: heat map of lipid species concentration. *B*: volcano plot of lipid class concentrations. CE, cholesteryl ester; CER, ceramide; DAG, diacylglycerol; DCER, dihydroceramide; FFA, free fatty acid; HCER, hexosylceramide; LCER, lactosylceramide; LPC, lysophosphatidylcholine; LPE, lysophosphatidylethanolamine; PC, phosphatidylcholine; PE, phosphatidylethanolamine; SM, sphingomyelin; TAG, triacylglycerol. *C*: lipid species composition of DCERs, CERs, LCERs, and HCERs of control (CTRL) and HSD17B12cKO (KO) males on *day 6* postinduction. *t* Test. Gray lines represent median values. ND, not detected. (CTRL, Cre−lox/lox, Tam, *n* = 5 mice; KO, Cre+ lox/lox, Tam, *n* = 5 mice.) **P* < 0.05, ***P* < 0.01.
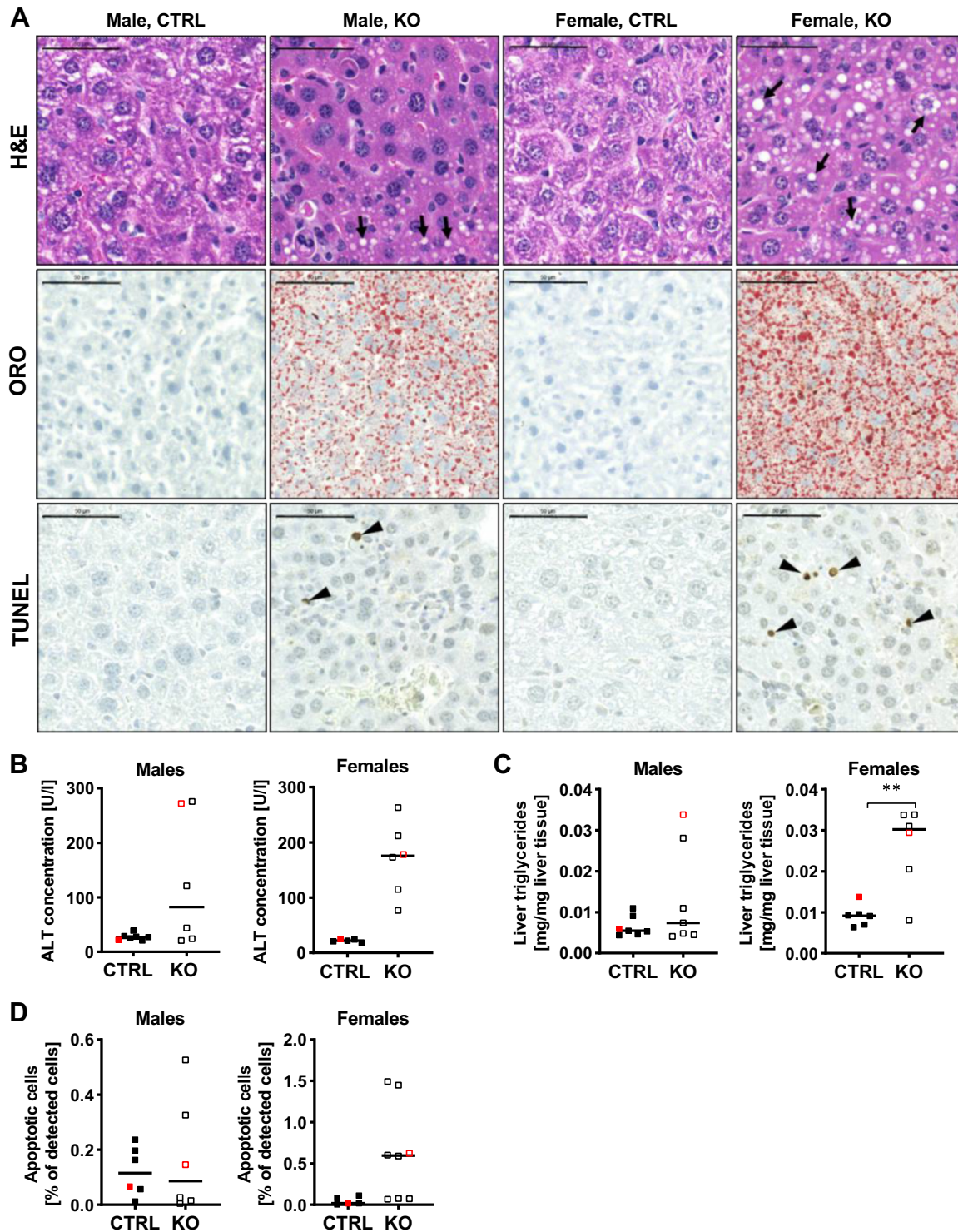
Fig. 5. Liver histology of conditional hydroxysteroid 17β dehydrogenase 12 knockout (HSD17B12cKO) of 10-wk-old male mice. Mice were euthanized on *day 6* after the induction of Cre recombination. *A*: hematoxylin-eosin (H&E; *top*), Oil Red O (ORO; *middle*), and terminal deoxynucleotidyl transferase dUTP nick end labeling (TUNEL) staining (*bottom*) of control (CTRL) and HSD17B12cKO (KO) male and female mice show microvesicular steatosis and apoptosis in the KO mice. The arrowheads indicate apoptotic cells, and arrows indicate lipid droplets. *B–D*: alanine aminotransferase (ALT) activity in serum (*B*), concentration of hepatic triglycerides (*C*), and percentage of apoptotic cells in the liver (*D*) on *day 6* after tamoxifen (Tam) induction of CTRL and KO mice. (Male CTRL, Cre− lox/lox, Tam, $n = 6$–7 mice; male KO, Cre+ lox/lox, Tam, $n = 6$ mice; female CTRL, Cre− lox/lox, Tam, $n = 5$–6 mice; female KO, Cre+ lox/lox, Tam, $n = 6$–8 mice.) Squares represent individual values, and horizontal lines represent median values. Red squares indicate the animal seen in the histological images. *t* Test. Scale bars, 50 μm.

ALT levels in HSD17B12cKO females and males, respectively, compared with control mice (Fig. 5*B*). In females, microvesicular steatosis was associated with a trend of increasing percentage of apoptotic cells in the HSD17B12cKO livers, indicating lipotoxic hepatocellular injury as well (Fig. 5*D*).

As the HSD17B12cKO mice showed signs of general toxicity and chronic pain with distress presented with piloerection, social isolation, partially closed eyelids, unresponsiveness, and snout grooming, we measured cytokines in serum to analyze their general inflammatory status. The data revealed a marked increase in IL-6, IL-17, and G-CSF levels in both male and female KO mice compared with the controls (Table 3). In addition, the data indicated a minor decrease in the levels of IP-10, IL-1α, and IL-5 in males and of MIP-1α, IFN-γ, and KC in females. These results further confirmed that the HSD17B12cKO mice suffered from systemic inflammation.

### Energy Depletion Leads to Reduced Hepatic De Novo Lipogenesis and Increased Gluconeogenesis in HSD17B12cKO Mice

The analysis of mRNA expression in liver samples of male mice 6 days after Tam induction did not indicate an enhanced FA uptake, as the mRNA expression for cluster of differentiation 36 (*Cd36*) and fatty acid transport protein 2 (*Fatp2*) was not altered (Supplemental Fig. S5). Neither was there a difference in mRNA expression for the proteins centrally involved in FA oxidation between the control and HSD17B12cKO mice. Those measured included peroxisome proliferator-activated receptor-α (*Ppara*), carnitine palmitoyl transferase 1 (*Cpt1a*), and acyl-CoA oxidase 1 (*Acox1*). However, of the mRNAs coding for the enzymes involved in FA esterification, diacylglycerol O-acyltransferase 1 (*Dgat1*) presented with a trend of higher expression in the HSD17B12cKO animals than in the control animals, whereas the mRNA expression of key enzymes involved in de novo lipogenesis, such as acetyl-CoA carboxylase-α (*Acaca*), fatty acid synthase (*Fasn*), and acyl-CoA desaturase 1 (*Scd1*), was decreased in the HSD17B12cKO mice compared with the controls.

PAS staining of liver sections 6 days after Tam induction showed reduced glycogen contents in the HSD17B12cKO livers compared with control livers. As a compensatory effect, mRNA expression for the enzyme presenting the rate-limiting step in gluconeogenesis, namely, phosphoenol-pyruvate carboxykinase (*Pepck*), was significantly increased in the HSD17B12cKO mice, and mRNA expression for *Pklr*, which encodes for a pyruvate kinase, was decreased in the KO animals. These results show that the hepatic glycogen stores of HSD17B12cKO mice were depleted 6 days after knockout induction and that the lipids accumulating within the hepatocytes were not of hepatic origin.

## DISCUSSION

In the present study, we generated an inducible conditional HSD17B12 KO mouse by crossing the HSD17B12-loxP mice with mice expressing tamoxifen-inducible Cre recombinase under the ubiquitously expressed ROSA26 locus (22, 58, 73). Our previous studies showed that HSD17B12 is essential for mouse embryonic development (46). In the current study, we showed that HSD17B12 activity is also essential for normal metabolic homeostasis in adult mice. The disruption of the HSD17B12 action led to a drastic loss of body weight within 6 days postinduction, evidenced by reduced fat and lean mass as well as severe dehydration. The weight loss was not observed in the adipocyte-specific HSD17B12cKO mouse model, indicating that despite the high expression of *Hsd17b12* in murine fat, the loss of stored fat was not due to disrupted HSD17B12 function in the adipose tissue.

During the first 5 days after tamoxifen induction the general well-being of HSD17B12cKO mice appeared normal, apart from weight loss. On *day 6*, we observed hunched posture, closed eyelids, and reduced locomotor activity, which are all signs of general illness and pain (8, 17, 18), and no studies beyond *day 6* postinduction were warranted. Similar signs are often observed in mouse models of sepsis (56) and in pathogen-induced sickness (35), as well as during cytotoxic chemotherapy (19, 48). The HSD17B12cKO mice seemed to have a trend of decreased locomotor activity already between *days 3* and *5*, but the difference observed was not significant. Furthermore, the HSD17B12cKO mice showed microsteatosis and increased triglyceride accumulation in the liver together with increased plasma ALT levels, which are all indicators of liver injury [6, 37, 68; for review, see Senior (55)]. Female mice are known to be more sensitive to toxicity compared with males (30, 31, 59). This is in line with the higher serum ALT levels in HSD17B12cKO females compared with the KO males. There was also a trend for increased apoptosis in female livers,

**Table 3.** *Cytokine concentrations measured in serum of HSD17B12cKO mice*

| | Males | | | | Females | | | |
|---|---|---|---|---|---|---|---|---|
| Cytokine | Control | HSD17B12cKO | FC | *P* Value | Control | HSD17B12cKO | FC | *P* Value |
| *n* | 10 | 10 | | | 9 | 10 | | |
| G-CSF | 511 ± 266 | 1,175 ± 299 | 2.30 | <0.001‡ | 628 ± 341 | 7,953 ± 3,753 | 12.6 | <0.001‡ |
| IFN-γ | 5.32 ± 2.02 | 4.38 ± 1.59 | −1.22 | ns | 6.10 ± 2.86 | 3.86 ± 2.36 | −1.58 | 0.028* |
| IL-1α | 417 ± 104 | 279 ± 87.9 | −1.50 | 0.005† | 228 ± 74.2 | 199 ± 114 | −1.15 | ns |
| IL-5 | 23.7 ± 17.6 | 10.0 ± 3.56 | −2.37 | 0.009† | 27.2 ± 6.29 | 20.9 ± 16.5 | −1.30 | ns |
| IL-6 | 7.43 ± 7.90 | 59.6 ± 48.9 | 8.02 | <0.001‡ | 5.35 ± 1.37 | 189 ± 125 | 35.3 | <0.001‡ |
| IL-17 | 20.44 ± 9.74 | 117.5 ± 96.2 | 5.75 | 0.005† | 35.75 ± 27.0 | 147.9 ± 88.1 | 4.14 | 0.001† |
| IP-10 | 481 ± 116 | 353 ± 121 | −1.36 | 0.026* | 391 ± 100 | 409 ± 209 | 1.05 | ns |
| KC | 710 ± 496 | 531 ± 477 | −1.34 | ns | 385 ± 186 | 1,756 ± 1,040 | 4.55 | 0.002† |
| MIP-1α | 32.1 ± 12.1 | 39.7 ± 20.3 | 1.24 | ns | 32.1 ± 8.87 | 20.9 ± 5.84 | −1.54 | 0.014* |

Values are means ± SD; *n* = no. of mice. Statistical significance was determined using the *t* test or nonparametric Mann–Whitney test depending on the normality of the data. FC, fold change; G-CSF, granulocyte colony-stimulating factor; HSD17B12cKO, conditional hydroxysteroid 17β dehydrogenase 12 knockout; IP-10, IFN-γ-induced protein 10; KC, keratinocyte chemoattractant; MIP-1α, macrophage inflammatory protein 1-α; ns, not significant. *$P < 0.05$, †$P < 0.01$, ‡$P < 0.001$, significantly different results.

but not in male livers. Thus, various indicative parameters for general well-being indicate that the mice with disrupted HSD17B12 enzyme suffer from general toxicity likely due to accumulation of toxic intermediates originating from the disrupted lipid metabolism.

The data indicated an increased level of proinflammatory cytokines, such as IL-6, IL-17, and G-CSF, in the HSD17B12cKO mice. IL-6 has been shown to induce cachexia by increasing lipolysis in WAT (25, 70). Furthermore, elevated serum IL-6 has been linked to weight loss in both patients with cancer cachexia (54) and patients with anorexia nervosa (15, 16). Thus, increased IL-6 is one potential mechanism for the weight loss observed in the HSD17B12cKO mice. The reduced lean mass and reduced glucose uptake in muscles in the HSD17B12cKO animals could be explained by elevated IL-6 as well, as high levels of IL-6 have been shown to induce muscle atrophy in animal models of cachexia [for review, see Dantzer and Kelley (18)]. It is still unclear how the lack of HSD17B12 leads to an increase in the levels of proinflammatory cytokines. However, our previous studies showed that disruption of HSD17B12 in mice leads to lower levels of prostanoids [PGD2, PGE2, PGF2a, and thromboxane $B_2$ (TXB2)] in ovaries (33). Prostanoids are involved in the regulation of cytokine production [for review, see Velasco et al. (63)]; low levels of prostaglandin E2 have been shown to increase IL-17 levels (49), and increased IL-17, in turn, is capable of inducing both IL-6 and G-CSF (12, 71), consequently promoting inflammation and sickness behavior.

HSD17B12 deficiency drastically reduced water and food intake in 3 days. Thus, the weight loss observed in HSD17B12cKO mice could be explained by the reduced food and water intake. Similarly, a fast for 48 h is sufficient to produce a weight loss of up to 20% of body weight in mice (20). Moreover, we did not observe any changes in the whole body energy expenditure in the KO mouse, suggesting that their general metabolism is not activated over that of the control mice. In a fasting state, the hypothalamic orexigenic peptide expressions of *Npy* and *Agrp* are known to increase, whereas anorexigenic *Pomc* mRNA expression is known to decrease to increase food intake and replenish energy stores (9, 13, 24, 50, 52, 53), and accordingly, this was also observed in HSD17B12cKO mice 6 days postinduction. This indicates that the hypothalamic regulation of hunger and satiety was responding to starvation in the HSD17B12cKO mice. Surprisingly, the *Hsd17b12* gene was still expressed in the brain, indicating that the 6-day-long time period following the Tam injection was not sufficient to induce Cre-mediated recombination in the brain. However, the anorexigenic *Crh* expression was increased in the KO mice. *Crh* is also a major regulator of the stress response (27), and administration of CRH is known to suppress appetite and cause anorexia in mice (5, 21, 62). Thus, the increased *Crh* expression in HSD17B12cKO mice in adulthood is in line with the observed stress response in the mice and, in addition to IL-6, could inhibit food intake.

In line with the heavily reduced adipose mass, serum lipid concentrations were mostly reduced in the HSD17B12cKO mice compared with controls. However, surprisingly, we observed an increased concentration of dihydroceramides in our KO model. Recent studies have found dihydroceramides to be regulators of autophagy in cell culture models of hepatic steatosis and cancer (28, 36). Furthermore, an increased ratio of dihydroceramides to ceramides has been shown to mediate apoptosis (28), and starvation is also known to induce autophagy (44, 47, 72). Thus, the increased dihydroceramide levels in HSD17B12cKO mice could contribute to the observed liver steatosis and inflammation. The lipidomics data also revealed a proportional increase in FA16-containing lipids in the HSD17B12cKO mice with an equivalent decrease in lipids including longer fatty acids (FA18, FA20, FA22, and FA24). This was also observed in cholesteryl esters, and to some extent in SMs (short ones accumulate, long ones did not change), but this proportional increase in shorter fatty acids was not observed in the FFA, LPC, LPE, PC, PE, or TAG classes. Together, these data suggest that HSD17B12 is essential for the normal composition of sphingomyelins and their precursors, i.e., ceramides and dihydroceramides.

Because of their heavily reduced food intake, the metabolic state of HSD17B12cKO mice at least partially resembles that of prolonged fasting. De novo lipogenesis appeared to be decreased, whereas gluconeogenesis was increased in the HSD17B12cKO mice, in line with previous studies on fasting response (40, 57). Defects in FA oxidation are a common cause behind fat accumulation in the hepatocytes in non-alcoholic fatty liver disease (NAFLD) [for review, see Mansouri et al. (38)]. However, this does not seem to be the mechanism for liver steatosis in the HSD17B12cKO mice. Of the other enzymes studied, DGAT1 preferably esterifies FAs imported to the cell, whereas DGAT2 utilizes FAs originating from de novo lipogenesis. Thus, the observed trend of induced *Dgat1* expression in the liver without a change in the *Dgat2* expression supports the idea of increased fat mobilization from adipose tissue in the HSD17B12cKO mice (45, 65, 69).

In conclusion, our KO mouse data show that HSD17B12 is essential for metabolic homeostasis in adult mice and *Hsd17b12* gene disruption leads to severe weight loss and liver steatosis. Mice with disrupted HSD17B12 enzyme suffer from general toxicity, possibly due to accumulation of toxic intermediates originating from the disrupted lipid metabolism or an imbalance in the production of prostaglandins and cytokines, leading to cytokine-induced sickness behavior. We suggest that the drastic loss of adipose tissue is largely due to an anorexia phenotype, potentially induced by the accumulation of toxic lipids. Further studies are needed to investigate the detailed mechanisms behind the severe inflammation and disrupted lipid homeostasis.

### DISCLOSURES

No conflicts of interest, financial or otherwise, are declared by the authors.

## AUTHOR CONTRIBUTIONS

## REFERENCES

1. **Adam M, Heikelä H, Sobolewski C, Portius D, Mäki-Jouppila J, Mehmood A, Adhikari P, Esposito I, Elo LL, Zhang FP, Ruohonen ST, Strauss L, Foti M, Poutanen M.** Hydroxysteroid (17β) dehydrogenase 13 deficiency triggers hepatic steatosis and inflammation in mice. *FASEB J* 32: 3434–3447, 2018. doi:10.1096/fj.201700914R.

2. **Bankhead P, Loughrey MB, Fernández JA, Dombrowski Y, McArt DG, Dunne PD, McQuaid S, Gray RT, Murray LJ, Coleman HG, James JA, Salto-Tellez M, Hamilton PW.** QuPath: open source software for digital pathology image analysis. *Sci Rep* 7: 16878, 2017. doi:10.1038/s41598-017-17204-5.

3. **Behan FM, Iorio F, Picco G, Gonçalves E, Beaver CM, Migliardi G, Santos R, Rao Y, Sassi F, Pinnelli M, Ansari R, Harper S, Jackson DA, McRae R, Pooley R, Wilkinson P, van der Meer D, Dow D, Buser-Doepner C, Bertotti A, Trusolino L, Stronach EA, Saez-Rodriguez J, Yusa K, Garnett MJ.** Prioritization of cancer therapeutic targets using CRISPR-Cas9 screens. *Nature* 568: 511–516, 2019. doi:10.1038/s41586-019-1103-9.

4. **Bellemare V, Phaneuf D, Luu-The V.** Target deletion of the bifunctional type 12 17β-hydroxysteroid dehydrogenase in mice results in reduction of androgen and estrogen levels in heterozygotes and embryonic lethality in homozygotes. *Horm Mol Biol Clin Investig* 2: 311–318, 2010. doi:10.1515/hmbci.2010.036.

5. **Benoit SC, Thiele TE, Heinrichs SC, Rushing PA, Blake KA, Steeley RJ.** Comparison of central administration of corticotropin-releasing hormone and urocortin on food intake, conditioned taste aversion, and c-Fos expression. *Peptides* 21: 345–351, 2000. doi:10.1016/S0196-9781(00)00153-4.

6. **Bernhard A, Rasinger JD, Wisløff H, Kolbjørnsen Ø, Secher Myrmel L, Berntssen MH, Lundebye AK, Ørnsrud R, Madsen L.** Subchronic dietary exposure to ethoxyquin dimer induces microvesicular steatosis in male BALB/c mice. *Food Chem Toxicol* 118: 608–625, 2018. doi:10.1016/j.fct.2018.06.005.

7. **Breitling R, Marijanović Z, Perović D, Adamski J.** Evolution of 17β-HSD type 4, a multifunctional protein of β-oxidation. *Mol Cell Endocrinol* 171: 205–210, 2001. doi:10.1016/S0303-7207(00)00415-9.

8. **Burkholder T, Foltz C, Karlsson E, Linton CG, Smith JM.** Health evaluation of experimental laboratory mice. *Curr Protoc Mouse Biol* 2: 145–165, 2012. doi:10.1002/9780470942390.mo110217.

9. **Chen SR, Chen H, Zhou JJ, Pradhan G, Sun Y, Pan HL, Li DP.** Ghrelin receptors mediate ghrelin-induced excitation of agouti-related protein/neuropeptide Y but not pro-opiomelanocortin neurons. *J Neurochem* 142: 512–520, 2017. doi:10.1111/jnc.14080.

10. **Chen Z, Kastaniotis AJ, Miinalainen IJ, Rajaram V, Wierenga RK, Hiltunen JK.** 17β-Hydroxysteroid dehydrogenase type 8 and carbonyl reductase type 4 assemble as a ketoacyl reductase of human mitochondrial FAS. *FASEB J* 23: 3682–3691, 2009. doi:10.1096/fj.09-133587.

11. **Chong J, Soufan O, Li C, Caraus I, Li S, Bourque G, Wishart DS, Xia J.** MetaboAnalyst 4.0: towards more transparent and integrative metabolomics analysis. *Nucleic Acids Res* 46: W486–W494, 2018. doi:10.1093/nar/gky310.

12. **Chung AS, Wu X, Zhuang G, Ngu H, Kasman I, Zhang J, Vernes JM, Jiang Z, Meng YG, Peale FV, Ouyang W, Ferrara N.** An interleukin-17-mediated paracrine network promotes tumor resistance to anti-angiogenic therapy. *Nat Med* 19: 1114–1123, 2013. doi:10.1038/nm.3291.

13. **Cowley MA, Smith RG, Diano S, Tschöp M, Pronchuk N, Grove KL, Strasburger CJ, Bidlingmaier M, Esterman M, Heiman ML, Garcia-Segura LM, Nillni EA, Mendez P, Low MJ, Sotonyi P, Friedman JM, Liu H, Pinto S, Colmers WF, Cone RD, Horvath TL.** The distribution and mechanism of action of ghrelin in the CNS demonstrates a novel hypothalamic circuit regulating energy homeostasis. *Neuron* 37: 649–661, 2003. doi:10.1016/S0896-6273(03)00063-1.

14. **Dai W, Liu H, Xu X, Ge J, Luo S, Zhu D, Amos CI, Fang S, Lee JE, Li X, Nan H, Li C, Wei Q.** Genetic variants in *ELOVL2* and *HSD17B12* predict melanoma-specific survival. *Int J Cancer* 145: 2619–2628, 2019. doi:10.1002/ijc.32194.

15. **Dalton B, Bartholdy S, Robinson L, Solmi M, Ibrahim MA, Breen G, Schmidt U, Himmerich H.** A meta-analysis of cytokine concentrations in eating disorders. *J Psychiatr Res* 103: 252–264, 2018. doi:10.1016/j.jpsychires.2018.06.002.

16. **Dalton B, Leppanen J, Campbell IC, Chung R, Breen G, Schmidt U, Himmerich H.** A longitudinal analysis of cytokines in anorexia nervosa. *Brain Behav Immun* 85: 88–95, 2020. doi:10.1016/j.bbi.2019.05.012.

17. **Dantzer R.** Cytokine, sickness behavior, and depression. *Immunol Allergy Clin North Am* 29: 247–264, 2009. doi:10.1016/j.iac.2009.02.002.

18. **Dantzer R, Kelley KW.** Twenty years of research on cytokine-induced sickness behavior. *Brain Behav Immun* 21: 153–160, 2007. doi:10.1016/j.bbi.2006.09.006.

19. **Elsea CR, Kneiss JA, Wood LJ.** Induction of IL-6 by cytotoxic chemotherapy is associated with loss of lean body and fat mass in tumor-free female mice. *Biol Res Nurs* 17: 549–557, 2015. doi:10.1177/1099800414558087.

20. **Enginar N, Nurten A, Türkmen AZ, Çağla B.** Scopolamine-induced convulsions in fasted animals after food intake: sensitivity of C57BL/6J mice and Sprague-Dawley rats. *Epilepsy Res* 112: 150–153, 2015. doi:10.1016/j.eplepsyres.2015.03.001.

21. **Fatima A, Andrabi S, Wolf G, Engelmann M, Spina MG.** Urocortin 1 administered into the hypothalamic supraoptic nucleus inhibits food intake in freely fed and food-deprived rats. *Amino Acids* 44: 879–885, 2013. doi:10.1007/s00726-012-1415-7.

22. **Friedrich G, Soriano P.** Promoter traps in embryonic stem cells: a genetic screen to identify and mutate developmental genes in mice. *Genes Dev* 5: 1513–1523, 1991. doi:10.1101/gad.5.9.1513.

23. **Gaiser RA, Pessia A, Ateeb Z, Davanian H, Fernández Moro C, Alkharaan H, Healy K, Ghazi S, Arnelo U, Valente R, Velagapudi V, Sällberg Chen M, Del Chiaro M.** Integrated targeted metabolomic and lipidomic analysis: a novel approach to classifying early cystic precursors to invasive pancreatic cancer. *Sci Rep* 9: 10208, 2019. doi:10.1038/s41598-019-46634-6.

24. **Hahn TM, Breininger JF, Baskin DG, Schwartz MW.** Coexpression of Agrp and NPY in fasting-activated hypothalamic neurons. *Nat Neurosci* 1: 271–272, 1998. doi:10.1038/1082.

25. **Han J, Meng Q, Shen L, Wu G.** Interleukin-6 induces fat loss in cancer cachexia by promoting white adipose tissue lipolysis and browning. *Lipids Health Dis* 17: 14, 2018. doi:10.1186/s12944-018-0657-0.

26. **He XY, Merz G, Mehta P, Schulz H, Yang SY.** Human brain short chain L-3-hydroxyacyl coenzyme A dehydrogenase is a single-domain multifunctional enzyme. Characterization of a novel 17β-hydroxysteroid dehydrogenase. *J Biol Chem* 274: 15014–15019, 1999. doi:10.1074/jbc.274.21.15014.

27. **Herman JP, McKlveen JM, Ghosal S, Kopp B, Wulsin A, Makinson R, Scheimann J, Myers B.** Regulation of the hypothalamic–pituitary–adrenocortical stress response. *Compr Physiol* 6: 603–621, 2016. doi:10.1002/cphy.c150015.

28. **Hernández-Tiedra S, Fabriàs G, Dávila D, Salanueva ÍJ, Casas J, Montes LR, Antón Z, García-Taboada E, Salazar-Roa M, Lorente M, Nylandsted J, Armstrong J, López-Valero I, McKee CS, Serrano-Puebla A, García-López R, González-Martínez J, Abad JL, Hanada K, Boya P, Goñi F, Guzmán M, Lovat P, Jäättelä M, Alonso A, Velasco G.** Dihydroceramide accumulation mediates cytotoxic autophagy of cancer cells via autolysosome destabilization. *Autophagy* 12: 2213–2229, 2016. doi:10.1080/15548627.2016.1213927.

29. **Horiguchi Y, Araki M, Motojima K.** 17β-Hydroxysteroid dehydrogenase type 13 is a liver-specific lipid droplet-associated protein. *Biochem Biophys Res Commun* 370: 235–238, 2008. doi:10.1016/j.bbrc.2008.03.063.

30. **Iimuro Y, Frankenberg MV, Arteel GE, Bradford BU, Wall CA, Thurman RG.** Female rats exhibit greater susceptibility to early alcohol-induced liver injury than males. *Am J Physiol Gastrointest Liver Physiol* 272: G1186–G1194, 1997. doi:10.1152/ajpgi.1997.272.5.G1186.

31. **Ikejima K, Enomoto N, Iimuro Y, Ikejima A, Fang D, Xu J, Forman DT, Brenner DA, Thurman RG.** Estrogen increases sensitivity of hepatic Kupffer cells to endotoxin. *Am J Physiol Gastrointest Liver Physiol* 274: G669–G676, 1998. doi:10.1152/ajpgi.1998.274.4.G669.

32. **Jokela H, Rantakari P, Lamminen T, Strauss L, Ola R, Mutka AL, Gylling H, Miettinen T, Pakarinen P, Sainio K, Poutanen M.** Hydrox-

ysteroid (17β) dehydrogenase 7 activity is essential for fetal de novo cholesterol synthesis and for neuroectodermal survival and cardiovascular differentiation in early mouse embryos. *Endocrinology* 151: 1884–1892, 2010. doi:10.1210/en.2009-0928.

33. **Kemiläinen H, Adam M, Mäki-Jouppila J, Damdimopoulou P, Damdimopoulos AE, Kere J, Hovatta O, Laajala TD, Aittokallio T, Adamski J, Ryberg H, Ohlsson C, Strauss L, Poutanen M.** The hydroxysteroid (17β) dehydrogenase family gene HSD17B12 is involved in the prostaglandin synthesis pathway, the ovarian function, and regulation of fertility. *Endocrinology* 157: 3719–3730, 2016. doi:10.1210/en.2016-1252.

34. **Kemiläinen H, Huhtinen K, Auranen A, Carpén O, Strauss L, Poutanen M.** The expression of HSD17B12 is associated with COX-2 expression and is increased in high-grade epithelial ovarian cancer. *Oncology* 94: 233–242, 2018. doi:10.1159/000485624.

35. **Kolmogorova D, Murray E, Ismail N.** Monitoring pathogen-induced sickness in mice and rats. *Curr Protoc Mouse Biol* 7: 65–76, 2017. doi:10.1002/cpmo.27.

36. **Lee AY, Lee JW, Kim JE, Mock HJ, Park S, Kim S, Hong SH, Kim JY, Park EJ, Kang KS, Kim KP, Cho MH.** Dihydroceramide is a key metabolite that regulates autophagy and promotes fibrosis in hepatic steatosis model. *Biochem Biophys Res Commun* 494: 460–469, 2017. doi:10.1016/j.bbrc.2017.10.110.

37. **Leung K, Quezada M, Chen Z, Kanel G, Kaplowitz N.** Niacin-induced anicteric microvesicular steatotic acute liver failure. *Hepatol Commun* 2: 1293–1298, 2018. doi:10.1002/hep4.1253.

38. **Mansouri A, Gattolliat CH, Asselah T.** Mitochondrial dysfunction and signaling in chronic liver diseases. *Gastroenterology* 155: 629–647, 2018. doi:10.1053/j.gastro.2018.06.083.

39. **Marchais-Oberwinkler S, Henn C, Möller G, Klein T, Negri M, Oster A, Spadaro A, Werth R, Wetzel M, Xu K, Frotscher M, Hartmann RW, Adamski J.** 17β-Hydroxysteroid dehydrogenases (17β-HSDs) as therapeutic targets: protein structures, functions, and recent progress in inhibitor development. *J Steroid Biochem Mol Biol* 125: 66–82, 2011. doi:10.1016/j.jsbmb.2010.12.013.

40. **Matsuda M, Korn BS, Hammer RE, Moon YA, Komuro R, Horton JD, Goldstein JL, Brown MS, Shimomura I.** SREBP cleavage-activating protein (SCAP) is required for increased lipid synthesis in liver induced by cholesterol deprivation and insulin elevation. *Genes Dev* 15: 1206–1216, 2001. doi:10.1101/gad.891301.

41. **Moon YA, Horton JD.** Identification of two mammalian reductases involved in the two-carbon fatty acyl elongation cascade. *J Biol Chem* 278: 7335–7343, 2003. doi:10.1074/jbc.M211684200.

42. **Nagasaki S, Miki Y, Akahira J, Suzuki T, Sasano H.** Transcriptional regulation of 17β-hydroxysteroid dehydrogenase type 12 by SREBP-1. *Mol Cell Endocrinol* 307: 163–168, 2009. doi:10.1016/j.mce.2009.04.002.

43. **Nagasaki S, Suzuki T, Miki Y, Akahira J, Kitada K, Ishida T, Handa H, Ohuchi N, Sasano H.** 17β-Hydroxysteroid dehydrogenase type 12 in human breast carcinoma: a prognostic factor via potential regulation of fatty acid synthesis. *Cancer Res* 69: 1392–1399, 2009. doi:10.1158/0008-5472.CAN-08-0821.

44. **Pietrocola F, Demont Y, Castoldi F, Enot D, Durand S, Semeraro M, Baracco EE, Pol J, Bravo-San Pedro JM, Bordenave C, Levesque S, Humeau J, Chery A, Métivier D, Madeo F, Maiuri MC, Kroemer G.** Metabolic effects of fasting on human and mouse blood in vivo. *Autophagy* 13: 567–578, 2017. doi:10.1080/15548627.2016.1271513.

45. **Qi J, Lang W, Geisler JG, Wang P, Petrounia I, Mai S, Smith C, Askari H, Struble GT, Williams R, Bhanot S, Monia BP, Bayoumy S, Grant E, Caldwell GW, Todd MJ, Liang Y, Gaul MD, Demarest KT, Connelly MA.** The use of stable isotope-labeled glycerol and oleic acid to differentiate the hepatic functions of DGAT1 and -2. *J Lipid Res* 53: 1106–1116, 2012. doi:10.1194/jlr.M020156.

46. **Rantakari P, Lagerbohm H, Kaimainen M, Suomela JP, Strauss L, Sainio K, Pakarinen P, Poutanen M.** Hydroxysteroid (17β) dehydrogenase 12 is essential for mouse organogenesis and embryonic survival. *Endocrinology* 151: 1893–1901, 2010. doi:10.1210/en.2009-0929.

47. **Rautou PE, Cazals-Hatem D, Moreau R, Francoz C, Feldmann G, Lebrec D, Ogier-Denis E, Bedossa P, Valla D, Durand F.** Acute liver cell damage in patients with anorexia nervosa: a possible role of starvation-induced hepatocyte autophagy. *Gastroenterology* 135: 840–848.e3, 2008. doi:10.1053/j.gastro.2008.05.055.

48. **Rix A, Drude N, Mrugalla A, Mottaghy FM, Tolba RH, Kiessling F.** Performance of severity parameters to detect chemotherapy-induced pain and distress in mice. *Laboratory Animals*. In press. doi:10.1177/0023677219883327.

49. **Saha A, Biswas A, Srivastav S, Mukherjee M, Das PK, Ukil A.** Prostaglandin E2 negatively regulates the production of inflammatory cytokines/chemokines and IL-17 in visceral leishmaniasis. *J Immunol* 193: 2330–2339, 2014. doi:10.4049/jimmunol.1400399.

50. **Sahu A.** Evidence suggesting that galanin (GAL), melanin-concentrating hormone (MCH), neurotensin (NT), proopiomelanocortin (POMC) and neuropeptide Y (NPY) are targets of leptin signaling in the hypothalamus. *Endocrinology* 139: 795–798, 1998. doi:10.1210/endo.139.2.5909.

51. **Sassmann A, Offermanns S, Wettschureck N.** Tamoxifen-inducible Cre-mediated recombination in adipocytes. *Genesis* 48: 618–625, 2010. doi:10.1002/dvg.20665.

52. **Schwartz MW, Seeley RJ, Campfield LA, Burn P, Baskin DG.** Identification of targets of leptin action in rat hypothalamus. *J Clin Invest* 98: 1101–1106, 1996. doi:10.1172/JCI118891.

53. **Schwartz MW, Seeley RJ, Woods SC, Weigle DS, Campfield LA, Burn P, Baskin DG.** Leptin increases hypothalamic pro-opiomelanocortin mRNA expression in the rostral arcuate nucleus. *Diabetes* 46: 2119–2123, 1997. doi:10.2337/diab.46.12.2119.

54. **Scott HR, McMillan DC, Crilly A, McArdle CS, Milroy R.** The relationship between weight loss and interleukin 6 in non-small-cell lung cancer. *Br J Cancer* 73: 1560–1562, 1996. doi:10.1038/bjc.1996.294.

55. **Senior JR.** Alanine aminotransferase: a clinical and regulatory tool for detecting liver injury-past, present, and future. *Clin Pharmacol Ther* 92: 332–339, 2012. doi:10.1038/clpt.2012.108.

56. **Shrum B, Anantha RV, Xu SX, Donnelly M, Haeryfar SM, McCormick JK, Mele T.** A robust scoring system to evaluate sepsis severity in an animal model. *BMC Res Notes* 7: 233, 2014. doi:10.1186/1756-0500-7-233.

57. **Sokolović M, Sokolović A, Wehkamp D, Ver Loren van Themaat E, de Waart DR, Gilhuijs-Pederson LA, Nikolsky Y, van Kampen AH, Hakvoort TB, Lamers WH.** The transcriptomic signature of fasting murine liver. *BMC Genomics* 9: 528, 2008. doi:10.1186/1471-2164-9-528.

58. **Soriano P.** Generalized *lacZ* expression with the ROSA26 Cre reporter strain. *Nat Genet* 21: 70–71, 1999. doi:10.1038/5007.

59. **Spruss A, Henkel J, Kanuri G, Blank D, Püschel GP, Bischoff SC, Bergheim I.** Female mice are more susceptible to nonalcoholic fatty liver disease: sex-specific regulation of the hepatic AMP-activated protein kinase-plasminogen activator inhibitor 1 cascade, but not the hepatic endotoxin response. *Mol Med* 18: 1346–1355, 2012. doi:10.2119/molmed.2012.00223.

60. **Stekhoven DJ, Bühlmann P.** MissForest: non-parametric missing value imputation for mixed-type data. *Bioinformatics* 28: 112–118, 2012. doi:10.1093/bioinformatics/btr597.

61. **Szajnik M, Szczepanski MJ, Elishaev E, Visus C, Lenzner D, Zabel M, Glura M, DeLeo AB, Whiteside TL.** 17β Hydroxysteroid dehydrogenase type 12 (HSD17B12) is a marker of poor prognosis in ovarian carcinoma. *Gynecol Oncol* 127: 587–594, 2012. doi:10.1016/j.ygyno.2012.08.010.

62. **Tanaka C, Asakawa A, Ushikai M, Sakoguchi T, Amitani H, Terashi M, Cheng K, Chaolu H, Nakamura N, Inui A.** Comparison of the anorexigenic activity of CRF family peptides. *Biochem Biophys Res Commun* 390: 887–891, 2009. doi:10.1016/j.bbrc.2009.10.069.

63. **Velasco C, Librán-Pérez M, Otero-Rodiño C, López-Patiño MA, Míguez JM, Soengas JL.** Ceramides are involved in the regulation of food intake in rainbow trout (*Oncorhynchus mykiss*). *Am J Physiol Regul Integr Comp Physiol* 311: R658–R668, 2016. doi:10.1152/ajpregu.00201.2016.

64. **Venkatesan R, Sah-Teli SK, Awoniyi LO, Jiang G, Prus P, Kastaniotis AJ, Hiltunen JK, Wierenga RK, Chen Z.** Insights into mitochondrial fatty acid synthesis from the structure of heterotetrameric 3-ketoacyl-ACP reductase/3R-hydroxyacyl-CoA dehydrogenase. *Nat Commun* 5: 4805, 2014. doi:10.1038/ncomms5805.

65. **Villanueva CJ, Monetti M, Shih M, Zhou P, Watkins SM, Bhanot S, Farese RV Jr.** Specific role for acyl CoA:diacylglycerol acyltransferase 1 (Dgat1) in hepatic steatosis due to exogenous fatty acids. *Hepatology* 50: 434–442, 2009. doi:10.1002/hep.22980.

66. **Visus C, Ito D, Dhir R, Szczepanski MJ, Chang YJ, Latimer JJ, Grant SG, DeLeo AB.** Identification of hydroxysteroid (17β) dehydrogenase type 12 (HSD17B12) as a CD8+ T-cell-defined human tumor antigen of human carcinomas. *Cancer Immunol Immunother* 60: 919–929, 2011. doi:10.1007/s00262-011-1001-y.

67. **Vooijs M, Jonkers J, Berns A.** A highly efficient ligand-regulated Cre recombinase mouse line shows that LoxP recombination is position dependent. *EMBO Rep* 2: 292–297, 2001. doi:10.1093/embo-reports/kve064.

68. **Weil JG, Bains C, Linke A, Clark DW, Stirnadel HA, Hunt CM.** Background incidence of liver chemistry abnormalities in a clinical trial population without underlying liver disease. *Regul Toxicol Pharmacol* 52: 85–88, 2008. doi:10.1016/j.yrtph.2008.06.001.

69. **Wurie HR, Buckett L, Zammit VA.** Diacylglycerol acyltransferase 2 acts upstream of diacylglycerol acyltransferase 1 and utilizes nascent diglycerides and de novo synthesized fatty acids in HepG2 cells. *FEBS J* 279: 3033–3047, 2012. doi:10.1111/j.1742-4658.2012.08684.x.

70. **Yao X, Huang J, Zhong H, Shen N, Faggioni R, Fung M, Yao Y.** Targeting interleukin-6 in inflammatory autoimmune diseases and cancers. *Pharmacol Ther* 141: 125–139, 2014. doi:10.1016/j.pharmthera.2013.09.004.

71. **Yao Z, Fanslow WC, Seldin MF, Rousseau AM, Painter SL, Comeau MR, Cohen JI, Spriggs MK.** Herpesvirus Saimiri encodes a new cyto-kine, IL-17, which binds to a novel cytokine receptor. *Immunity* 3: 811–821, 1995. doi:10.1016/1074-7613(95)90070-5.

72. **Yao Z, Zhou H, Figeys D, Wang Y, Sundaram M.** Microsome-associated lumenal lipid droplets in the regulation of lipoprotein secretion. *Curr Opin Lipidol* 24: 160–170, 2013. doi:10.1097/MOL.0b013e32835aebe7.

73. **Zambrowicz BP, Imamoto A, Fiering S, Herzenberg LA, Kerr WG, Soriano P.** Disruption of overlapping transcripts in the ROSA β geo 26 gene trap strain leads to widespread expression of β-galactosidase in mouse embryos and hematopoietic cells. *Proc Natl Acad Sci USA* 94: 3789–3794, 1997. doi:10.1073/pnas.94.8.3789.

74. **Zhi X, Wang J, Lu P, Jia J, Shen HB, Ning G.** AdipoCount: a new software for automatic adipocyte counting. *Front Physiol* 9: 85, 2018. doi:10.3389/fphys.2018.00085.